Published as: *Nature*. 2013 November 7; 503(7474): 72–77.

SHANK3 overexpression causes manic-like behavior with unique pharmacogenetic properties

Kihoon Han[1,2,8], **J. Lloyd Holder Jr.**[3,4,8], **Christian P. Schaaf**[1,8], **Hui Lu**[1,2,8], **Hongmei Chen**[3,7,8], **Hyojin Kang**[1,8,9], **Jianrong Tang**[3,8], **Zhenyu Wu**[3,8], **Shuang Hao**[3,8], **Sau Wai Cheung**[1,6], **Peng Yu**[1,8], **Hao Sun**[3,7,8], **Amy M. Breman**[1,6], **Ankita Patel**[1,6], **Hui-Chen Lu**[3,5,7,8], and **Huda Y. Zoghbi**[1,2,3,5,8]

[1]Department of Molecular and Human Genetics, Baylor College of Medicine, Houston, TX 77030, USA.

[2]Howard Hughes Medical Institute, Baylor College of Medicine, Houston, TX 77030, USA.

[3]Departments of Pediatrics, Baylor College of Medicine, Houston, TX 77030, USA.

[4]Division of Neurology and Developmental Neuroscience, Baylor College of Medicine, Houston, TX 77030, USA.

[5]Program in Developmental Biology and Department of Neuroscience, Baylor College of Medicine, Houston, TX 77030, USA.

[6]Medical Genetics Laboratories, Baylor College of Medicine, Houston, TX 77030, USA.

[7]The Cain Foundation Laboratories, Houston, TX 77030, USA.

[8]Jan and Dan Duncan Neurological Research Institute at Texas Children's Hospital, Houston, TX 77030, USA.

Abstract

Mutations in *SHANK3* and large duplications of the region spanning *SHANK3* both cause a spectrum of neuropsychiatric disorders, suggesting that proper *SHANK3* dosage is critical for normal brain function. *SHANK3* overexpression *per se* has not been established as a cause of human disorders, however, because 22q13 duplications involve several genes. Here we report that *Shank3* transgenic mice modeling a human *SHANK3* duplication exhibit manic-like behavior and seizures consistent with synaptic excitatory/inhibitory imbalance. We also identified two patients with hyperkinetic disorders carrying the smallest *SHANK3*-spanning duplications reported so far. These findings suggest *SHANK3* overexpression causes a hyperkinetic neuropsychiatric disorder.

Correspondence and requests for materials should be addressed to H.Y.Z. (hzoghbi@bcm.edu).
[9]Present address: National Institute of Supercomputing and Networking, Korea Institute of Science and Technology Information, Daejeon, Korea

Author Contributions K.H., J.L.H., H.L., H.C., J.T., H.-C.L. and H.Y.Z. designed the experiments. K.H., J.L.H., H.L., H.C., J.T., Z.W., S.H. and H.S. performed the research. K.H., J.L.H., C.P.S., H.L., H.C., H.K., J.T., Z.W., S.H., S.W.C., P.Y., A.M.B., A.P., H.-C.L. and H.Y.Z. collected, analyzed and interpreted the data. K.H., J.L.H., C.P.S., H.L., H.K., J.T., H.-C.L. and H.Y.Z. wrote and edited the paper.

The authors declare no competing financial interests. Readers are welcome to comment on the online version of the paper.

To probe the mechanism underlying the phenotype, we generated a Shank3 *in vivo* interactome and found that Shank3 directly interacts with the Arp2/3 complex to increase F-actin levels in *Shank3* transgenic mice. The mood-stabilizing drug valproate, but not lithium, rescues the manic-like behavior of *Shank3* transgenic mice raising the possibility that this hyperkinetic disorder has a unique pharmacogenetic profile.

An increasing number of neuropsychiatric disorders such as autism spectrum disorder (ASD), intellectual disability (ID), schizophrenia, obsessive-compulsive disorder and bipolar disorder are being classified as "synaptopathies"[1–4], because the genes mutated in these disorders lead to abnormal synaptic development or function. For example, all members of the *SHANK* gene family (*SHANK1*, *2* and *3*), which encode for core scaffolding proteins organizing macromolecular complexes at the postsynaptic density (PSD)[5], have been linked to human synaptopathies[6–8]. Point mutations in *SHANK3* (also called *ProSAP2*) are seen in non-syndromic autism, ID and schizophrenia[8–12], and deletions of the region containing *SHANK3* cause Phelan-McDermid syndrome (22q13 deletion syndrome)[13,14]. Furthermore, mice modeling *SHANK3* deletion mirror the human behavioral phenotypes and display synaptic abnormalities[15–17].

Interestingly, a few 22q13 duplications spanning *SHANK3* have been reported in patients diagnosed with Asperger syndrome, attention deficit-hyperactivity disorder (ADHD) or schizophrenia[9,10,18], suggesting that increased expression of *SHANK3* could be also deleterious. Because duplication cases involve large genomic regions (>0.8 Mb) with more than 20 genes, however, it is unclear if it is *SHANK3* overexpression that causes a neurological phenotype. Here, we describe the generation and characterization of *Shank3*-overexpressing mice and on the role of *SHANK3* duplication in hyperkinetic neuropsychiatric disorders in humans. We identify a mechanism that contributes to the neuronal phenotype and report pharmacological therapies that might benefit individuals with *SHANK3* overexpression.

Manic-like behavior in *Shank3* TG mice

We introduced an N-terminal EGFP-tag into mouse *Shank3* to generate *EGFP-Shank3* transgenic (TG) mice (Fig. 1a and Extended Data Fig. 1a). Similar to endogenous *Shank3*[16], *EGFP-Shank3* transcript was detected in cortex, hippocampus and striatum (Fig. 1b). The regional and developmental expression of EGFP-Shank3 recapitulated those of endogenous Shank3 (Extended Data Fig. 1b–d). EGFP-Shank3 was targeted to the dendritic spines and co-localized with excitatory postsynaptic marker PSD-95, but not with inhibitory postsynaptic marker Gephyrin (Fig. 1c). Compared to wild-type (WT) mice, TG mice expressed 1.2 to 2-fold higher levels of each of the three major Shank3 isoforms (α, β and γ), with ~50% more total Shank3 protein (Fig. 1d and Extended Data Fig. 1e, f), which parallels expression in human *SHANK3* duplication patients. There was no significant change in levels of other synaptic proteins in the hippocampus and striatum of TG mice (Extended Data Fig. 1g, h).

Our *Shank3* TG mice showed increased locomotor activity and speed compared with WT littermates in the open field test (Fig. 2a, b and Extended Data Fig. 2a). TG mice were also

hyperactive in their home cages, suggesting that their behavior in the open field was not due to the novel environment (Extended Data Fig. 2b). Given that one patient carrying a large 22q13 duplication spanning *SHANK3* has been reported to have ADHD[10], we sought to determine whether the hyperactivity in the TG mice is related to ADHD by testing whether it could be corrected by amphetamine, a treatment for ADHD. Surprisingly, rather than the expected paradoxical calming effect, an acute injection of amphetamine aggravated the hyperactivity of TG mice to a greater degree than WT mice (Fig. 2c, d). As increased sensitivity to amphetamine is one characteristic of mania[19]—bipolar disorder can be misdiagnosed as ADHD, especially in children due to the overlap in diagnostic criteria[20]—we pursued behavioral tests to determine if there are abnormalities typically associated with a manic state.

Immobility during the tail-suspension test has been used as an indicator of despair. Consistent with manic-like behavior[21], the duration of immobility in *Shank3* TG mice was less than WT littermates (Fig. 2e); the TG mice also exhibited elevated acoustic startle response with reduced prepulse inhibition (PPI), abnormal circadian rhythms, and hyperphagia-like behavior (Fig. 2f–j and Extended Data Fig. 2c, d), all of which are behaviors observed in humans during manic episodes[22,23].

We normalized Shank3 levels by crossing the TG mice with *Shank3B*$^{+/-}$ mice[16] and found that this reversed hyperactivity, reduced immobility in tail-suspension, and reduced PPI (Extended Data Fig. 3). *Shank3* TG mice also displayed decreased social interaction (Extended Data Fig. 2e–g), which has also been seen in patients with large 22q13 duplications[9,18]. Unlike *Shank3* knockout mice[16,17], *Shank3* TG mice did not exhibit repetitive behavior (Extended Data Fig. 2h–j), but they made fewer calls during the ultrasonic vocalization test at postnatal day 13 (Extended Data Fig. 2k, l). Together, these results suggest that ~50% increase in Shank3 level causes a hyperkinetic phenotype in mice that resembles mania, and that it is the increased dosage of *SHANK3* in 22q13 duplications that likely contributes to hyperkinesia in humans.

SHANK3 duplications in humans

To confirm unequivocally the role of *SHANK3* dosage in the neuropsychiatric phenotypes, we queried the array Comparative Genomic Hybridization (aCGH) database at the Molecular Genetics Laboratory of Baylor College of Medicine and identified two cases that carry small duplications (Fig. 3a, b and Supplementary Information 1).

The first individual is an 11-year old girl diagnosed with ADHD, combined type. The 22q13 duplication includes the entire *SHANK3* and part of the *ACR* gene (Fig. 3a). *ACR* encodes acrosin, a protease expressed in sperm facilitating its penetration into oocytes, with no known expression or function in brain. This individual has seizures and exhibits hyperactivity, poor attention, auditory overstimulation, hyperphagia and kleptomania. Notably, her hyperactivity is resistant to the paradoxical calming effect of stimulant medications seen in most cases of ADHD. The second individual is a 35-year old man diagnosed with bipolar disorder and epilepsy who has a duplication encompassing *SHANK3*, *ACR*, and *ARSA*, the gene encoding arylsulfatase A (Fig. 3b). *ARSA* deficiency causes

metachromatic leukodystrophy, and duplications of *ARSA* have not been associated with any neurobehavioral phenotype.

These two individuals carry the smallest 22q13 duplications spanning *SHANK3* reported so far, and their molecular and clinical findings support the notion that *SHANK3* duplications result in hyperkinetic disorders and seizures in humans. More detailed clinical and molecular cytogenetic information about both individuals is provided in the supplementary material.

Synaptic E/I imbalance in *Shank3* TG mice

Having found that humans with *SHANK3* duplications have a hyperkinetic disorder and seizures, we evaluated the *Shank3* TG mice for seizures and synaptic abnormalities. We observed spontaneous seizures in the *Shank3* TG mice, but never in WT littermates (Supplementary Video 1). We monitored for electrographic seizures using electroencephalography (EEG). The EEG of TG mice showed hyperexcitability discharges accompanied by electrographic seizures (Fig. 4a). Since alteration in the neuronal excitatory/inhibitory (E/I) balance is considered to cause seizures[24], we examined morphological and functional changes of both excitatory and inhibitory synapses. Cultured hippocampal pyramidal neurons from TG mice displayed increased VGLUT1-positive PSD-95, an excitatory synaptic marker, and decreased VGAT-positive Gephyrin, an inhibitory synaptic marker, puncta density (Fig. 4b).

We examined functional properties of synapses by whole-cell patch clamping in CA1 pyramidal neurons of acute hippocampal slices. Neuronal density, paired-pulse facilitation ratio, input-output relationship, and intrinsic excitability of these neurons were similar in WT and TG mice, suggesting normal basal synaptic transmission at Schaffer collateral-CA1 synapses of TG mice (Extended Data Fig. 4a–e). Consistent with decreased density of VGAT-positive Gephyrin puncta in cultured hippocampal neurons from TG mice, we observed reduction in $GABA_A$ receptor-mediated miniature inhibitory postsynaptic current (mIPSC) frequency, but not in amplitude or decay time (Fig. 4c). AMPA receptor-mediated miniature EPSC (mEPSC) was normal, but amplitude of spontaneous EPSC (sEPSC, without TTX) was increased in TG mice (Extended Data Fig. 4f and Fig. 4d). There was no change in AMPA/NMDA ratio in CA1 pyramidal neurons of TG mice compared to WT mice (Fig. 4e). Consistently, NMDA receptor-dependent synaptic plasticity measured by extracellular field recordings at Schaffer collateral–CA1 pyramidal synapses was normal in TG mice (Extended Data Fig. 4g, h). The spontaneous seizures of TG mice, together with morphological and functional alterations in synapses, suggest the synaptic E/I balance in TG neurons is shifted toward excitation.

Arp2/3 complex mediates F-actin increase

To understand the molecular mechanisms underlying the synaptic alterations of *Shank3* TG mice, we set out to identify the *in vivo* interactors of Shank3. We used the EGFP-tag of the *Shank3* transgene to isolate Shank3 protein complexes (Extended Data Fig. 5a). Immunoprecipitation (IP) followed by mass-spectrometry analysis identified 273 proteins that bind Shank3 *in vivo* (Supplementary Table 4). There was significant overlap between the proteins on this list, those from our previous Y2H screening[25], and known mouse or

human PSD proteins[26,27] (Extended Data Fig. 5b). We combined our two Shank3-focused experimental lists (previous Y2H screening[25] and current *in vivo* IP, for a total 404 proteins called Shank3 interactome) for further analysis (Extended Data Fig. 5c, d).

We performed Gene Ontology (GO) and pathway analysis, which suggested that regulation of actin cytoskeleton is a principal role of the Shank3 interacting proteins (Extended Data Fig. 5e and Supplementary Table 5). Based on this analysis, we hypothesized that abnormal regulation of the actin cytoskeleton could be one major molecular change in the synapses of TG mice. Accordingly, we evaluated the effects of a 50% increase in Shank3 on F-actin levels. We found that F-actin levels of excitatory synapses were increased by ~30% in cultured hippocampal pyramidal neurons from TG mice compared to WT mice (Fig. 5a), which was restored by expression of *Shank3* siRNA (Extended Data Fig. 6a, b). Next, we utilized our Shank3 interactome to generate a sub-network of actin-related proteins (Fig. 5b) to focus the search on molecular mediators of the elevated F-actin. This network comprises both known and novel Shank3 interactors, which we confirmed by western blotting (Extended Data Fig. 5f). The most interesting new Shank3 direct interactors we identified (based on both Y2H screening and *in vivo* IP) were two subunits of the Arp2/3 complex (ARPC2 and ARPC5L) (Fig. 5b). Arp2/3 complex consists of seven-subunits and binds directly to the F-actin mother filament to initiate nucleation and branching[28]. Consistent with the interaction analysis, ARPC2 clusters co-localized with EGFP-Shank3 and significantly enlarged in TG neurons (Extended Data Fig. 5g and Fig. 5c); the latter observation was reversed by *Shank3* siRNA (Extended Data Fig. 6c). To initiate actin polymerization, Arp2/3 complex must be activated by nucleation-promoting factors (NPFs)[28]. Given that the NPFs WASF1 and Cortactin (CTTN) directly interact with Shank3[29,30], Shank3 could function as a scaffold that brings WASF1, Cortactin and Arp2/3 together, facilitating the formation of F-actin structures (Fig. 5d). Consistent with our hypothesis, co-localization of WASF1 and ARPC2 was enhanced in TG neurons (Fig. 5e). Furthermore, the density of dendritic spines was increased in TG brains compared to WT brains (Fig. 5f).

Our analysis suggested hippocampal pyramidal neurons of TG mice have a reduced number of inhibitory synapses (Fig. 4b, c), which was unexpected based on the exclusive localization of EGFP-Shank3 in excitatory synapses (Fig. 1c). To understand the underlying mechanism, we first investigated inhibitory neurons, changes of which might secondarily affect inhibitory synapses on pyramidal neurons. However, we found that there was no difference in synapse number on the GAD-6-positive inhibitory neurons of TG mice, although these neurons express EGFP-Shank3 (Extended Data Fig. 7).

We next explored a possible cell-autonomous relationship between excitatory and inhibitory synapses of TG pyramidal neurons. We hypothesized that increased clustering of actin-related proteins in excitatory synapses might reduce some of those proteins in inhibitory synapses, thereby contributing to the decrease of inhibitory synapse number. We focused on actin-related proteins, since the actin cytoskeleton defines the molecular architecture of both E/I synapses[31]. We picked Mena and Profilin as candidates for four reasons: they directly interact with Gephyrin in inhibitory synapses[32]; Profilin1 and Profilin2 are recruited to excitatory synapses by neuronal activity[33,34]; Profilin2 was also identified in our Shank3 *in*

vivo IP (Supplementary Table 4); and Mena and Profilin interact with proteins in the Shank3 interactome (Extended Data Fig. 8). Both proteins showed decreased localization to inhibitory synapses, and Profilin2 showed enhanced localization to excitatory synapses in TG neurons (Fig. 5g–i). Together, these results suggest that increased expression of Shank3 enhances F-actin levels through Arp2/3 complex in excitatory synapses of TG neurons. By modulating the synaptic distributions of Mena and Profilin2, this contributes, at least in part, to changes in inhibitory synapses.

Shank3 TG mice respond to valproate

Having established that Shank3 overexpression causes mania-like behavior in mice and a hyperkinetic syndrome in humans, we tested whether mood-stabilizing drugs for human mania could rescue the behavioral abnormalities of TG mice. First, we examined the effect of lithium, the first FDA-approved treatment for bipolar disorder, which inhibits multiple targets including inositol monophosphatase and glycogen synthase kinase-3 (GSK-3)[35]. The basal activity of GSK-3β in TG mouse hippocampus and striatum was similar to that of WT mice (Fig. 6a). Mice were fed with lithium carbonate-containing chow for three weeks, resulting in serum lithium levels (WT: 0.82 ± 0.04, TG: 0.91 ± 0.08 mmol/L) comparable to those in the therapeutic range for humans (0.6~1.2 mmol/L). Lithium did not mitigate any of the manic-like behaviors of *Shank3* TG mice (Fig. 6b and Extended Data Fig. 9).

Given that our mice display seizures in addition to manic-like behavior, we decided to test valproate, another FDA-approved mood-stabilizing drug used to treat manic or mixed episodes that also acts as an anticonvulsant, increases GABA neurotransmission and inhibits sodium channels, calcium channels and histone deacetylase 1[36]. We treated the TG mice with acute intraperitoneal injections of either valproate (200 mg/kg) or saline and subjected them to behavioral testing. Valproate reversed the baseline hyperactivity, the amphetamine-hypersensitivity (Fig. 6c, d), and the abnormal acoustic startle response and PPI (Fig. 6e–h) in TG mice. The behavior of WT mice, except for a decrease in baseline activity and an increase of PPI in male mice, was not significantly affected by valproate treatment (Fig. 6c–h). Valproate also significantly decreased the frequency of epileptiform spikes in TG mice as measured by EEG (Fig. 6i). Valproate treatment changed neither the levels of synaptic proteins in hippocampus or striatum of WT and TG mice, nor F-actin levels in cultured hippocampal neurons of TG mice (Extended Data Fig. 10).

Discussion

There are multiple genomic loci for which both deletions and duplications cause human neuropsychiatric disorders, suggesting that proper dosage of some genes is critical for normal brain function[37,38]. In most cases, however, the genes causing the respective phenotypes are poorly defined, making it hard to understand pathogenesis and to develop targeted therapies. Chromosome 22q13 spanning *SHANK3* is one example. Although *SHANK3* loss has been shown to cause ASD in humans, *SHANK3* overexpression has never been definitively determined to cause neuropsychiatric disease. In this study, we generated *Shank3* TG mice that model a human duplication and identified patients with the smallest 22q13 duplications involving *SHANK3*. The remarkable similarity of the neurobehavioral

phenotypes between the mouse model and patients with *SHANK3* duplications supports the notion that *SHANK3* overexpression causes a hyperkinetic neuropsychiatric disorder that approximates mania. Indeed, either a 50% reduction or 50% increase in Shank3 levels results in marked neuropsychiatric phenotypes and a predisposition to epilepsy.

Notably, the manic-like behavior of *Shank3* TG mice was reversed selectively by valproate but not by lithium treatment. It is not uncommon to find human patients with bipolar disorder (BPD) that are resistant to lithium monotherapy[39]. Indeed, a subset of individuals with the rapid-cycling form of BPD is highly resistant to lithium[40]. As GSK-3 is considered the major target for lithium's efficacy in the treatment of BPD[41], the lithium-resistance of *Shank3* TG mice and their normal GSK-3β activity are congruent with a mechanism independent of GSK-3 and possibly more dependent upon synaptic alterations, including E/I imbalance.

Synaptic E/I imbalance is likely to underlie the pathogenesis for seizures[24,42] and a broad spectrum of neuropsychiatric disorders[1,43]. We found morphological and functional changes in E/I synapses of TG neurons favoring excitation, which might account for both seizures and hyperkinetic behavior. Consistent with this, GABAergic dysfunction in patients with bipolar disorder has been reported[44], and valproate (which increases GABA neurotransmission and decreases high-frequency action potential firing) rescued the manic-like behaviors of TG mice. In contrast, lithium enhances excitatory postsynaptic potentials in CA1 synapses[45], which might explain the resistance of *Shank3* TG mice to lithium treatment. Mechanistically, enhanced F-actin polymerization through Arp2/3 complex could be responsible for the synaptic changes of TG neurons, but other Shank3-dependent molecular pathways cannot be excluded.

In conclusion, our study advances our understanding of the human diseases associated with *SHANK3* and the mechanisms that can lead to bipolar disorder. We propose two distinct mechanisms leading to bipolar disorder: one is dysfunction of the well-established GSK-3 pathway that is responsive to lithium treatment; the second is a synaptic dysfunction associated with an E/I balance shifted toward excitation, which could result in hyperkinetic behaviors, and which is resistant to lithium but sensitive to valproate. We believe this sort of pharmacogenetic analysis in model organisms could improve treatment strategies for patients with bipolar disorder as the genetic underpinnings of each patient's illness are elucidated.

Online-only Methods

Generation of *Shank3* transgenic mice

To generate *Shank3* transgenic mice, we used a BAC clone (RP23-278D8) containing a segment of mouse chromosome 15. This BAC clone was modified by recombineering techniques[46] to insert Kozak sequence (ACCATGG) followed by EGFP sequence (cloned from pEGFP-C1) at the first start codon of *Shank3* gene (exon 1). The modified BAC clone was double digested with NotI/SwaI, and the ~75 kb linearized segment with entire *Shank3* gene plus ~12 kb 5' and ~2 kb 3' was injected into the FVB/N embryos (Extended Data Fig. 1a). The primers used for genotyping were designed against EGFP sequence (forward: 5'-

atggtgagcaagggcgaggag-3', reverse: 5'-gcggacttgaagaagtcgtgc-3'). All procedures to maintain and use these mice were approved by the Institutional Animal Care and Use Committee for Baylor College of Medicine.

Primary antibodies

Antibodies used for the western blots and/or immunostainings are Akt (Cell Signaling Technology; 4691), phospho-Akt (Thr308) (Cell Signaling Technology; 2965), Arpc2 (Millipore; 07-227), β-actin (Abcam; ab20272), CYFIP2 (Abcam; ab95969), $GABA_AR$ β3 (NeuroMab; 75-149), GAD-6 (Developmental Studies Hybridoma Bank), Gephyrin (Synaptic Systems; 147 111), GFP (Abcam; ab290, ab13970), GKAP (NeuroMab; 75-156), GluR2 (NeuroMab; 75-002), GSK-3α/β (Millipore; 05-412), phospho-GSK-3β (Ser9) (Cell Signaling Technology; 9336), Homer (Santa Cruz; sc-15321), MAP2 (Sigma; M9942), Mena/Vasp (Millipore; MAB2635), mGluR5 (Millipore; AB5675), NR1 (Millipore; MAB363), Profilin2 (TU-Braunschweig; 4H5), PSD-95 (NeuroMab; 75-028), pan-Shank (3856; Choi et al., 2005[47]), Shank1 (NeuroMab; 75-064), Shank2 (NeuroMab; 75-088), Shank3 (Santa Cruz; H-160), VGAT (Synaptic Systems; 131 002), VGlut1 (Synaptic Systems; 135 302) and WASF1 (NeuroMab; 75-048).

Preparation of brain lysates and western blot

S2 (soluble fraction) and P2 (crude synaptosomal fraction) subcellular, and PSD fractions (synaptic fraction after one time Triton X-100 washout) were prepared as described[48]. For Akt and GSK-3 detection, brains were dissected and homogenized in ice-cold lysis buffer (20 mM Tris-HCl, pH 7.4, 150 mM NaCl, 2 mM EDTA, 1% Tx-100, 10% glycerol with protease and phosphatase inhibitor (Roche)). Western blot images were acquired by LAS 4000 (GE Healthcare), and quantified by an ImageJ software package.

Hippocampal neuron cultures, transfection and immunostaining

Hippocampal neurons were prepared from postnatal day 0–1 FVB/N mice and plated on poly-D-lysine/mouse laminin coated coverslips (BD biosciences) in Neurobasal medium supplemented with GlutaMAX-I (Invitrogen), B-27 and 1% FBS. At DIV 7, neurons were tranfected with pEGFP-C1 plus either control or *Shank3* siRNA (Ambion, s81603 or s81605). At DIV 14, neurons were fixed with 4% formaldehyde/4% sucrose in PBS, and permeabilized with 0.2% Tx-100 in PBS. PBS with 0.1% BSA and 3% horse serum was used for blocking and antibody incubation. Alexa-conjugated phalloidin (Invitrogen) was used to visualize F-actin. Z-stack images were acquired by LSM710 (Zeiss) confocal microscope under the same parameter settings, and the images were quantified in blind manner using ImageJ.

RNA In situ hybridization

Hybridization probe specific for EGFP sequence was prepared by PCR amplification from the pEGFP-C1 using the following primers (forward: 5'-atggtgagcaagggcgaggag-3', reverse: 5'-cttgtacagctcgtccatgcc-3'). Riboprobe was generated using DIG RNA Labeling Mix (Roche).

Golgi staining

Standard Golgi-Cox impregnation using the FD Rapid Golgistain kit (NeuroTechnologies) was performed with brains from 10-week-old FVB/N male mice. Serial sagittal sections (50 μm) were collected and images of dendritic spines on the secondary branches (apical dendrites of CA1 pyramidal neurons) were acquired by LSM710 (Zeiss) confocal microscope under DIC mode. The images were quantified in blind manner using ImageJ.

Cresylviolet staining

Brains from 10-week-old FVB/N male mice were cryosectioned (25 μm) and stained with 0.2% cresyl violet.

Drug treatment

For each experiment, individual was blinded to genotype and littermates were randomly distributed to control and treatment groups as follows; Animal with genotype A was assigned to control, next animal of genotype A to drug, third to control. Same with genotype B. Amphetamine and valproate (Sigma) were dissolved in normal saline to final concentration of 0.2 g/L and 20 g/L, respectively. Mice received intraperitoneal injection of amphetamine (2 mg/kg), valproate (200 mg/kg) or saline in a volume of 10 ml/kg. Valproate was injected three times before each behavioral assay (10 a.m. and 5 p.m. of a day before, and 9 a.m. of the day of assay), and assays were performed 30 min after final injection. For lithium treatment, mice were fed either lithium carbonate-containing chow or control chow (Harlan Teklad). The lithium group was initially fed 0.2% lithium carbonate chow for a week followed by 0.4% chow for two more weeks before the behavioral assays. Water with 0.85% sodium chloride was provided to counteract toxicity of lithium. Lithium concentration in serum was measured using lithium assay kit (Crystal Chem, Inc.) according to the manufacturer's instruction.

Behavioral assays

All data acquisition and analyses were carried out by an individual blinded to the genotype. For behavioral assays, 2-3-months-old mice (both males and females) of the F1 hybrid (FVB/N × C57BL/6J) were used to mitigate strain specific effects. A sample size of mice was chosen to mitigate genetic background variance. Before each test, mice were habituated in the test room at least for 30 min. Mice with sign of seizures (before, during or after test) were excluded from the analysis. The summary of statistical analysis for behavioral assays is provided in Supplementary Table 1.

Open field

After habituated in the test room (600 lux, 60 dB white noise), mice were placed in the center of a clear, open Plexiglass chamber (40 × 40 × 30 cm), and the activities were measured by photobeam breaks (Accuscan, Columbus, OH) for 30 min. To measure amphetamine response, mice received intraperitoneal injection of saline or amphetamine after 30 min test of basal activities, and the activities were measured for additional 60 min.

Home-cage activity

Single-caged mice were habituated in the cage for 12 hr, and the activities were measured by photobeam breaks (Accuscan, Columbus, OH) for 48 hr under the light cycle of 07:00–19:00.

Tail suspension

After habituation period in the test room (600 lux, 60 dB white noise), mice were suspended by their tails. Movements were recorded and the immobile time was automatically measured by ANY-maze software (Stoelting Co.). The same parameter setting for the definition of immobility was applied for all the mice tested.

Acoustic startle response and prepulse inhibition

Mice were placed in a test chamber (San Diego Instruments) and habituated for 5 min with 70 dB background white noise. Eight trial types (no stimulus, a 40 ms 120 dB sound as the startle stimulus, and three different prepulse sounds (20 ms 74, 78, 82 dB) either alone or 100 ms before the startle stimulus) were presented in pseudo-random order with six times per each trial type. The interval between each trial type was 10 to 20 s. The maximum startle amplitude during the 65 ms period following the onset of the startle stimulus was used to calculate percentage prepulse inhibition.

Circadian rhythms

Mice were individually housed in cages equipped with a 11.5 cm diameter wheel, and wheel-running activity was recorded by VitalView software (Respironics Mini-Mitter system). Mice were held on a 12:12 light/dark cycle for 8 to 14 days with food, water and temperature at 20 ± 2 °C. Mice were then released into constant dark for 14 days.

Three chamber test

The test was performed as previously described[49]. The three chamber apparatus is a clear Plexiglass box (24.75 × 16.75 × 8.75 in) with removable partitions separating the box into left, center and right chambers. The age- and gender-matched C57BL/6J mice were used as novel partners. Two days before the test, the novel partner mice were habituated to the wire cages (3 in diameter × 4 in height) for 1 hour per day. The wire cage with inanimate novel object inside served as a control. The test mouse was habituated in the chamber for 15 min as described[49]. During the habituation period, neither wild-type nor *Shank3* transgenic mice showed a preference for either side of the chamber (data not shown). After the habituation period, the novel partner mouse was placed into one of the wire cages and located randomly in either the right or left side of chamber. The novel object was placed into the wire cage located in the other side of chamber. The test mouse was allowed to explore the three chamber apparatus for 15 min. The movements were recorded and the total amount of time spent in each chamber was automatically measured by ANY-maze software (Stoelting Co.). The close interaction time, defined by rearing, sniffing or pawing at each wire cage, was measured manually.

Grooming

After habituation period in the test room (600 lux, 60 dB white noise), mice were placed into the center of Plexiglass cylinder (20 cm in diameter × 30 cm in height) and videotaped for 10 min. The amount of time spent grooming was measured from the videotape.

Ultrasonic vocalization

Separation-induced ultrasonic vocalizations (USV) were measured on pups of postnatal day 6 to 13. A standard housing cage containing one female and her offspring was transferred to a holding room and allowed to acclimate for 30 min. Following this acclimation period, the cage was transferred to a testing room. Pups were placed into a clean and warm (35 °C) cage and allowed to acclimate for 5 min. The mother was removed from the testing room and transferred back to the holding room. After 5 min acclimation period, one pup will be placed individually into a plastic beaker in a testing chamber. A bat detector positioned 10 cm above the beaker transduced ultrasonic signals. USV was quantified for a total testing period of 2 min using sound analysis software (Ultravox, Noldus Information Technology).

Electrophysiology

EEG measurement

All data acquisition and analyses were carried out blinded to genotype. FVB/N male mice of 2-3-months-old were anesthetized with isoflurane. Under aceptic condition, each mouse was surgically implanted with tungsten electrodes (50 μm diameter) aimed at hippocampal CA1 (P2.0R1.2H1.3) and dentate (P2.0R1.8H1.8) regions. The third EEG electrode made of silver wire (127 μm diameter) was implanted in the subdural space of the right frontal cortex area. A reference/grounding electrode was then positioned in the occipital region of the skull. All electrode wires were attached to a miniature connector (Harwin Connector). After 3–5 days of post-surgical recovery, EEG activities (filtered between 0.1 Hz and 5 kHz, sampled at 10 kHz) were recorded for 1 hour per day over 3–5 days. In the experiments evaluating the effects of valproate on EEG activities, adult male *Shank3* TG mice with implanted electrode went through recording sessions for 3 consecutive days. On each day, animals received one hour baseline recording before valproate (200 mg/kg, i.p.) followed by another hour of post recording.

EEG data analysis

Electrographic seizure time lasting over 10 s was counted manually and normalized as the percentage of the total recording period. The number of abnormal epileptiform spikes were counted using Clampfit 10 software (Molecular Devices, LLC) when the sharp positive deflections exceeding twice the baseline and lasting 25–100 ms[50]. In the pharmacological tests, spike numbers were normalized to the baseline value before drug administration in day 1.

Whole-cell patch-clamp recordings

All data acquisition and analyses were carried out blinded to genotype. Acute fresh hippocampal slices were prepared from FVB/N male mice at the age of 6–8 weeks old as

previously described[51]. Coronal slices (250 μm thick) containing medial hippocampus were cut with a vibratome (Leica Microsystems Inc) in a chamber filled with chilled (2–5 °C) cutting solution containing (in mM) 110 choline-chloride, 25 $NaHCO_3$, 25 D-glucose, 11.6 sodium ascorbate, 7 $MgSO_4$, 3.1 sodium pyruvate, 2.5 KCl, 1.25 NaH_2PO_4 and 0.5 $CaCl_2$. The slices were then incubated in artificial cerebrospinal fluid (ACSF, in mM) containing 119 NaCl, 26.2 $NaHCO_3$, 11 D-glucose, 3 KCl, 2 $CaCl_2$, 1 $MgSO_4$, 1.25 NaH_2PO_4 at the room temperature. The solutions were bubbled with 95% O_2 and 5% CO_2. Whole-cell recording was made using patchclamp amplifiers (Multiclamp 700B) under infrared–differential interference contrast microscopy (Zeiss). Data acquisition and analysis were performed using digitizers (DigiData 1440A) and analysis software pClamp 10 (Molecular Devices). Signals were filtered at 2 kHz and sampled at 10 kHz. Spontaneous EPSCs (sEPSCs), miniature EPSCs (mEPSCs) and IPSCs (mIPSCs) were recorded from CA1 hippocampal pyramidal neurons at −70 mV in voltage-clamp mode. sEPSCs were recorded in the presence of $GABA_A$ receptor blocker, SR95531 (10 μM). mEPSCs were recorded in the presence of tetrodotoxin (TTX, 0.5 μM) and SR95531 (10 μM). Glass pipettes with a resistance of 2.5-5 MΩ were filled with a solution containing (in mM) 140 potassium gluconate, 5 KCl, 10 HEPES, 0.2 EGTA, 2 $MgCl_2$, 4 MgATP, 0.3 Na_2GTP and 10 Na_2-phosphocreatine, pH 7.2 (with KOH). For recording mIPSCs, potassium gluconate was replaced with KCl (140 μM) in the pipette solution. Besides TTX (0.5 μM), glutamate receptor antagonists 6-cyano-7-nitroquinoxaline-2,3-dione disodium (CNQX) (10 μM) and D-2-amino-5-phosphonovaleric acid (D-AP-5) (25 μM) were also added to the bath. Series resistance (15–30 MΩ) and input resistance (100–200 MΩ) were monitored throughout the whole-cell recording. Evoked EPSCs were recorded in the presence of SR95531 (10 μM). To stimulate presynaptic inputs, stimulation pulses (50 μs duration at 0.1 Hz) were applied to a bipolar tungsten stimulation electrode (WPI Inc., Sarasota, FL) placed along the Schaffer collaterals. Extracellular stimuli were administered using a stimulator system (Master 8, Jerusalem, Israel). The stimulating and recording pipettes were placed at the same depth in the slice and the distance between them was kept constant (~300 μm). Data were discarded when the change in the series resistance was >20% during the course of the experiment. The whole-cell recording was performed at (30 ± 1) °C with the help of an automatic temperature controller (Warner Instr.). For measurements of the AMPA-to-NMDA receptor ratio, the CA1 pyramidal neuron was voltage-clamped at 40mV. First, a stable baseline recording of total EPSCs was obtained. The NMDA receptor antagonist D-AP-5 (50 mM) was then applied to the bath for 5–10 min to isolate fast AMPA-receptor-mediated EPSCs. Digital subtraction of AMPA-receptor-EPSCs from the total EPSCs from the same neuron yielded NMDA-receptor-EPSCs. An average of 12–20 EPSCs were collected for each type of EPSC. The bath solution contained picrotoxin (100 μM). The intracellular solution contained 140mM $CsCH_3SO_3$, 10mM HEPES, 1 mM EGTA, 5mM TEA-Cl, 2mM $MgCl_2$, 2.5mM MgATP and 0.3mM GTP, pH7.2–7.4 (with CsOH).

Extracellular field recordings

All data acquisition and analyses were carried out blinded to genotype. 1–2 months old FVB/N male mice were anesthetized with isoflurane and their brains were removed and immersed immediately in ice-cold cutting solution (in mM): 110 sucrose, 3 KCl, 0.5 $CaCl_2$, 60 $NaCl_2$, 7 $MgCl_2$, 1.25 NaH_2PO4, 28 $NaHCO_3$, 5 D-glucose saturated with 95% O_2 and

5% CO_2. 400 μm thick transverse hippocampal slices were prepared with a vibrating microtome Series 1000 (Vibratome Company, St. Louis, MO) and recovered at 31 ± 0.5 °C for an hour in an interface chamber. Field excitatory postsynaptic potential (fEPSP) were recorded at 31 ± 0.5 °C in an interface chamber perfused at 1 ml/min with artificial cerebrospinal fluid (ACSF) containing (in mM): 125 NaCl, 2.5 KCl, 2 $CaCl_2$, 1 $MgCl_2$, 1.25 NaH_2PO_4, 25 $NaHCO_3$, and 15 D-glucose. Extracellular stimuli were administered along the Schaffer collaterals using Formvar-insulated, bipolar nichrome electrodes controlled by a stimulus isolator (A-M Systems, Carlsborg, WA). An ACSF-filled glass-recording electrode was placed in *stratum radiatum* to record the field potential changes. Electrophysiological traces were amplified with AC-coupled amplifier (model 1800; A-M Systems), digitized using a Digidata 1320A (Molecular Devices, Union City, CA), and acquired with pClamp 10 software (Molecular Devices). To assess baseline synaptic transmission, input-output relationships were examined by measuring the rising slope of the fEPSP evoked by 100 μs pulses over various stimulus intensities (1V to 10V). The stimulation intensity that evoked a fEPSP whose slope was 30–40% of the maximum fEPSP slope, determined by the input-output recording experiment, was used for the following recording paradigms. Long-term potentiation (LTP) was induced by two trains of 100 stimuli pulses at 100 Hz that are separated 20 sec apart. To monitor LTP development, the fEPSPs were recorded every 20 seconds for 20 minutes before and 60 minutes after induction. The magnitude of potentiation was determined by measuring the changes in the slope of the fEPSP. NMDAR-dependent long-term depression (LTD) formation was induced with 900 paired stimuli with 50 msec inter-stimulus interval at 1 Hz frequency. In all experiments, genotypes will be confirmed by PCR with tails cut. All data are shown as mean ± s.e.m.

In vivo IP and mass-spectrometry

Striatum and hippocampus were dissected from 8 animals (5-week-old) per each genotype (wild-type and *Shank3* transgenic FVB/N male mice), and crude synaptosomal fraction solubilized with deoxycholic acid (DOC) buffer was prepared as described previously[47]. ~10 mg of lysates were incubated with GFP-Trap beads (ChromoTek) for 2 hr at 4 °C. The beads were briefly washed with Binding/Dialysis buffer (50 mM Tris-HCl, pH 7.4, 0.1% Triton X-100) and boiled in with 1X NUPAGE LDS sample buffer (Invitrogen) to be loaded on SDS-PAGE (NuPAGE 4–12% Bis-Tris Gel, Invitrogen). The eluted proteins were visualized with Coomassie Brilliant blue-stain and excised into 10 gel pieces according to molecular size. The individual gel pieces were destained and subject to in-gel digestion using trypsin. Tryptic peptide was dissolved in 10 μl of loading solution (5% methanol containing 0.1% formic acid) and subjected to nanoflow LC-MS/MS analysis with a nano-LC II (Thermo Scientific) coupled to LTQ Orbitrap Velos (Thermo Scientific) mass spectrometer. The peptides were loaded onto an in-housed Reprosil-Pur Basic C18 (3 μm, Dr.Maisch GmbH, Germany) trap column which was 2 cm × 75 um size. Then the trap column was washed with loading solution and switched in-line with an in-housed 100 mm × 75 um column packed with Reprosil-Pur Basic C18 equilibrated in 0.1% formic acid/water. The peptides were separated with a 75 min discontinuous gradient of 5–28% acetonitrile/0.1% formic acid at a flow rate of 450 nl/min. Separated peptides were directly electro-sprayed into LTQ Orbitrap Velos mass spectrometer. The LTQ Orbitrap instrument was operated in the data-dependant mode acquiring fragmentation spectra of the top 50 strongest

ions and under direct control of Xcalibur software (Thermo Scientific). Obtained MS/MS spectra were searched against target-decoy mouse refseq database in Proteome Discoverer 1.3 interface (Thermo Fisher) with Mascot algorithm (Mascot 2.3, Matrix Science). The precursor mass tolerance was confined within 20 ppm with fragment mass tolerance of 0.5 dalton and a maximum of two missed cleavage allowed. Assigned peptides were filtered with 5% false discover rate (FDR) and subject to manual verifications. Any protein whose peptide was identified from wild-type brain sample was excluded from the further analysis.

Bioinformatics

Construction of Shank3 interactome network

To build an interaction network with the union set of Shank3 interactors (*in vivo* IP plus Y2H screening), protein interactions were adopted from iRefIndex database (http://irefindex.uio.no) which provides consolidated protein interactions from the 10 primary interaction databases (BIND, BioGRID, CORUM, DIP, HPRD, IntAct, MINT, MPact, MPPI and OPHID). Only the interactions among human and mouse genes were included. The direct interactions were distinguished from the indirect interactions based on experimental assays. Network graphics were generated with Cytoscape[52]. Nodes and edges were colored based on the source and interaction type of the proteins, respectively. Thickness of edges for direct interactions correlates with the number of supportive evidences in the interaction database (Fig. 5b). To simplify the network, orphan nodes, defined by the nodes which have interaction only with Shank3, were excluded from the network (Extended Data Fig. 5c).

Network topology analysis of Shank3 interactome

Shortest path length (the number of links of the shortest path traveling from one protein to another protein) was calculated to measure the network topology of Shank3 interactome. To test the significance, we randomly picked same number of proteins from the mouse PSP[26] and calculated shortest path length of the interactome network generated with the proteins. This re-sampling was repeated 10,000 times and the empirical *P* value (the number of sample networks whose mean path length is smaller than that of Shank3 interactome/10,000) was calculated.

Gene Ontology analysis

The gene ontology (GO) analysis was carried out using DAVID software (version 6.7)[53,54]. The union set of Shank3 interactors from the *in vivo* IP and Y2H screening was tested against a customized background gene list where low expressed genes in mouse brain were excluded.

Human Subjects

Both individuals were referred to the Medical Genetics Laboratories, Baylor College of Medicine, Houston, USA, for clinical array comparative genomic hybridization (aCGH) analysis. Following informed consent, approved by the Institutional Review Board for Human Subject Research at Baylor College of Medicine, the medical records of the

respective individuals were reviewed. Additional clinical information was obtained by phone interview with patient 1's legal guardian and patient 2, respectively.

Array Comparative Genomic Hybridization

Patient DNA, isolated from peripheral whole blood using the Puregene DNA extraction kit (Gentra, Minneapolis, MN, USA) following the manufacturer's instructions, was analyzed using the Baylor College of Medicine V8 OLIGO clinical genomic microarray, described in Boone *et al*. Briefly, this is a custom-designed genomic microarray with both genome-wide coverage and supplemental exonic coverage of ~1700 known or suspected disease genes, including *SHANK3*.

Quantification and Statistical analysis

For quantification, values from three independent experiments with at least three biological replicates were used. For behavioral assays, all population values appear normally distributed and the variance is similar between the groups. *P* values were calculated by Student's *t* test or analysis of variance with proper post-hoc tests (GraphPad Prism), as specified in each figure legend or Supplementary Table 1–3. All data are presented as mean ± s.e.m. **P*<0.05; ***P*<0.01; ****P*<0.001.

Supplementary Material

Refer to Web version on PubMed Central for supplementary material.

Acknowledgements

We are indebted to the patients and families who participated in this study; to Dr. John W Belmont (Baylor College of Medicine, Houston, TX) and Dr. Nicole Miller (Mountain States Medical Group Pediatrics, Kingsport, TN) for contributing patients to this study; Dr. Guoping Feng (MIT) for sharing *Shank3B* mice; Gabriele Schuster for injection of *Shank3* BAC; and Corinne Spencer for behavioral assays training. This project was supported by The Howard Hughes Medical Institute (H.Y.Z.), NIH ARRA grant (1R01NS070302) (H.Y.Z.), the Baylor Intellectual and Developmental Disabilities Research Center (P30HD024064) confocal, electrophysiology and mouse neurobehavioral cores, and the Cancer Prevention and Research Institute of Texas (CPRIT) RP110784. J.L.H. was supported by an Early Career Award from the Thrasher Research Fund, NIH 2T32NS043124 and the Ting Tsung and Wei Fong Chao Foundation; C.P.S. was supported by the Joan and Stanford Alexander family, the Ting Tsung and Wei Fong Chao Foundation and the Doris Duke Clinical Scientist Development Award.

References

1. Sudhof TC. Neuroligins and neurexins link synaptic function to cognitive disease. Nature. 2008; 455:903–911. [PubMed: 18923512]
2. Zoghbi HY. Postnatal neurodevelopmental disorders: meeting at the synapse? Science. 2003; 302:826–830. [PubMed: 14593168]
3. Bourgeron T. A synaptic trek to autism. Curr Opin Neurobiol. 2009; 19:231–234. [PubMed: 19545994]
4. Ting JT, Peca J, Feng G. Functional consequences of mutations in postsynaptic scaffolding proteins and relevance to psychiatric disorders. Annu Rev Neurosci. 2012; 35:49–71. [PubMed: 22540979]
5. Sheng M, Kim E. The Shank family of scaffold proteins. J Cell Sci. 2000; 113(Pt 11):1851–1856. [PubMed: 10806096]
6. Sato D, et al. SHANK1 Deletions in Males with Autism Spectrum Disorder. Am J Hum Genet. 2012; 90:879–887. [PubMed: 22503632]

7. Berkel S, et al. Mutations in the SHANK2 synaptic scaffolding gene in autism spectrum disorder and mental retardation. Nat Genet. 2010; 42:489–491. [PubMed: 20473310]
8. Grabrucker AM, Schmeisser MJ, Schoen M, Boeckers TM. Postsynaptic ProSAP/Shank scaffolds in the cross-hair of synaptopathies. Trends Cell Biol. 2011; 21:594–603. [PubMed: 21840719]
9. Durand CM, et al. Mutations in the gene encoding the synaptic scaffolding protein SHANK3 are associated with autism spectrum disorders. Nat Genet. 2007; 39:25–27. [PubMed: 17173049]
10. Moessner R, et al. Contribution of SHANK3 mutations to autism spectrum disorder. Am J Hum Genet. 2007; 81:1289–1297. [PubMed: 17999366]
11. Gauthier J, et al. Novel de novo SHANK3 mutation in autistic patients. Am J Med Genet B Neuropsychiatr Genet. 2009; 150B:421–424. [PubMed: 18615476]
12. Gauthier J, et al. De novo mutations in the gene encoding the synaptic scaffolding protein SHANK3 in patients ascertained for schizophrenia. Proc Natl Acad Sci U S A. 2010; 107:7863–7868. [PubMed: 20385823]
13. Bonaglia MC, et al. Disruption of the ProSAP2 gene in a t(12;22)(q24.1;q13.3) is associated with the 22q13.3 deletion syndrome. Am J Hum Genet. 2001; 69:261–268. [PubMed: 11431708]
14. Bonaglia MC, et al. Identification of a recurrent breakpoint within the SHANK3 gene in the 22q13.3 deletion syndrome. J Med Genet. 2006; 43:822–828. [PubMed: 16284256]
15. Bozdagi O, et al. Haploinsufficiency of the autism-associated Shank3 gene leads to deficits in synaptic function, social interaction, and social communication. Mol Autism. 2010; 1:15. [PubMed: 21167025]
16. Peca J, et al. Shank3 mutant mice display autistic-like behaviours and striatal dysfunction. Nature. 2011; 472:437–442. [PubMed: 21423165]
17. Wang X, et al. Synaptic dysfunction and abnormal behaviors in mice lacking major isoforms of Shank3. Hum Mol Genet. 2011; 20:3093–3108. [PubMed: 21558424]
18. Failla P, et al. Schizophrenia in a patient with subtelomeric duplication of chromosome 22q. Clin Genet. 2007; 71:599–601. [PubMed: 17539913]
19. Shaltiel G, et al. Evidence for the involvement of the kainate receptor subunit GluR6 (GRIK2) in mediating behavioral displays related to behavioral symptoms of mania. Mol Psychiatry. 2008; 13:858–872. [PubMed: 18332879]
20. Leibenluft E, Rich BA. Pediatric bipolar disorder. Annu Rev Clin Psychol. 2008; 4:163–187. [PubMed: 17716034]
21. Martinowich K, Schloesser RJ, Manji HK. Bipolar disorder: from genes to behavior pathways. J Clin Invest. 2009; 119:726–736. [PubMed: 19339764]
22. Perry W, Minassian A, Feifel D, Braff DL. Sensorimotor gating deficits in bipolar disorder patients with acute psychotic mania. Biol Psychiatry. 2001; 50:418–424. [PubMed: 11566158]
23. Belmaker RH. Bipolar disorder. N Engl J Med. 2004; 351:476–486. [PubMed: 15282355]
24. McCormick DA, Contreras D. On the cellular and network bases of epileptic seizures. Annu Rev Physiol. 2001; 63:815–846. [PubMed: 11181977]
25. Sakai Y, et al. Protein interactome reveals converging molecular pathways among autism disorders. Sci Transl Med. 2011; 3 86ra49.
26. Collins MO, et al. Molecular characterization and comparison of the components and multiprotein complexes in the postsynaptic proteome. J Neurochem. 2006; 97(Suppl 1):16–23. [PubMed: 16635246]
27. Bayes A, et al. Characterization of the proteome, diseases and evolution of the human postsynaptic density. Nat Neurosci. 2011; 14:19–21. [PubMed: 21170055]
28. Campellone KG, Welch MD. A nucleator arms race: cellular control of actin assembly. Nat Rev Mol Cell Biol. 2010; 11:237–251. [PubMed: 20237478]
29. Proepper C, et al. Abelson interacting protein 1 (Abi-1) is essential for dendrite morphogenesis and synapse formation. Embo J. 2007; 26:1397–1409. [PubMed: 17304222]
30. Naisbitt S, et al. Shank, a novel family of postsynaptic density proteins that binds to the NMDA receptor/PSD-95/GKAP complex and cortactin. Neuron. 1999; 23:569–582. [PubMed: 10433268]
31. Sheng M, Kim E. The postsynaptic organization of synapses. Cold Spring Harb Perspect Biol. 2011; 3

32. Giesemann T, et al. Complex formation between the postsynaptic scaffolding protein gephyrin, profilin, and Mena: a possible link to the microfilament system. J Neurosci. 2003; 23:8330–8339. [PubMed: 12967995]
33. Neuhoff H, et al. The actin-binding protein profilin I is localized at synaptic sites in an activity-regulated manner. Eur J Neurosci. 2005; 21:15–25. [PubMed: 15654839]
34. Ackermann M, Matus A. Activity-induced targeting of profilin and stabilization of dendritic spine morphology. Nat Neurosci. 2003; 6:1194–1200. [PubMed: 14555951]
35. Jope RS. Anti-bipolar therapy: mechanism of action of lithium. Mol Psychiatry. 1999; 4:117–128. [PubMed: 10208444]
36. Rosenberg G. The mechanisms of action of valproate in neuropsychiatric disorders: can we see the forest for the trees? Cell Mol Life Sci. 2007; 64:2090–2103. [PubMed: 17514356]
37. Ramocki MB, Zoghbi HY. Failure of neuronal homeostasis results in common neuropsychiatric phenotypes. Nature. 2008; 455:912–918. [PubMed: 18923513]
38. Toro R, et al. Key role for gene dosage and synaptic homeostasis in autism spectrum disorders. Trends Genet. 2010; 26:363–372. [PubMed: 20609491]
39. Gitlin M. Treatment-resistant bipolar disorder. Mol Psychiatry. 2006; 11:227–240. [PubMed: 16432528]
40. Dunner DL, Fieve RR. Clinical factors in lithium carbonate prophylaxis failure. Arch Gen Psychiatry. 1974; 30:229–233. [PubMed: 4589148]
41. Gould TD, Manji HK. Glycogen synthase kinase-3: a putative molecular target for lithium mimetic drugs. Neuropsychopharmacology. 2005; 30:1223–1237. [PubMed: 15827567]
42. Magloczky Z, Freund TF. Impaired and repaired inhibitory circuits in the epileptic human hippocampus. Trends Neurosci. 2005; 28:334–340. [PubMed: 15927690]
43. Marin O. Interneuron dysfunction in psychiatric disorders. Nat Rev Neurosci. 2012; 13:107–120. [PubMed: 22251963]
44. Benes FM, et al. Regulation of the GABA cell phenotype in hippocampus of schizophrenics and bipolars. Proc Natl Acad Sci U S A. 2007; 104:10164–10169. [PubMed: 17553960]
45. Schloesser RJ, Martinowich K, Manji HK. Mood-stabilizing drugs: mechanisms of action. Trends Neurosci. 2012; 35:36–46. [PubMed: 22217451]

References

46. Warming S, Costantino N, Court DL, Jenkins NA, Copeland NG. Simple and highly efficient BAC recombineering using galK selection. Nucleic Acids Res. 2005; 33:e36. [PubMed: 15731329]
47. Choi J, et al. Regulation of dendritic spine morphogenesis by insulin receptor substrate 53, a downstream effector of Rac1 and Cdc42 small GTPases. J Neurosci. 2005; 25:869–879. [PubMed: 15673667]
48. Han K, et al. Regulated RalBP1 binding to RalA and PSD-95 controls AMPA receptor endocytosis and LTD. PLoS Biol. 2009; 7:e1000187. [PubMed: 19823667]
49. Chao HT, et al. Dysfunction in GABA signalling mediates autism-like stereotypies and Rett syndrome phenotypes. Nature. 2010; 468:263–269. [PubMed: 21068835]
50. Roberson ED, et al. Amyloid-beta/Fyn-induced synaptic, network, and cognitive impairments depend on tau levels in multiple mouse models of Alzheimer's disease. The Journal of neuroscience : the official journal of the Society for Neuroscience. 2011; 31:700–711. [PubMed: 21228179]
51. Lu H, Lim B, Poo MM. Cocaine exposure in utero alters synaptic plasticity in the medial prefrontal cortex of postnatal rats. J Neurosci. 2009; 29:12664–12674. [PubMed: 19812341]
52. Shannon P, et al. Cytoscape: a software environment for integrated models of biomolecular interaction networks. Genome Res. 2003; 13:2498–2504. [PubMed: 14597658]
53. Dennis G Jr. et al. DAVID: Database for Annotation, Visualization, and Integrated Discovery. Genome Biol. 2003; 4:P3. [PubMed: 12734009]
54. Huang da W, Sherman BT, Lempicki RA. Systematic and integrative analysis of large gene lists using DAVID bioinformatics resources. Nat Protoc. 2009; 4:44–57. [PubMed: 19131956]

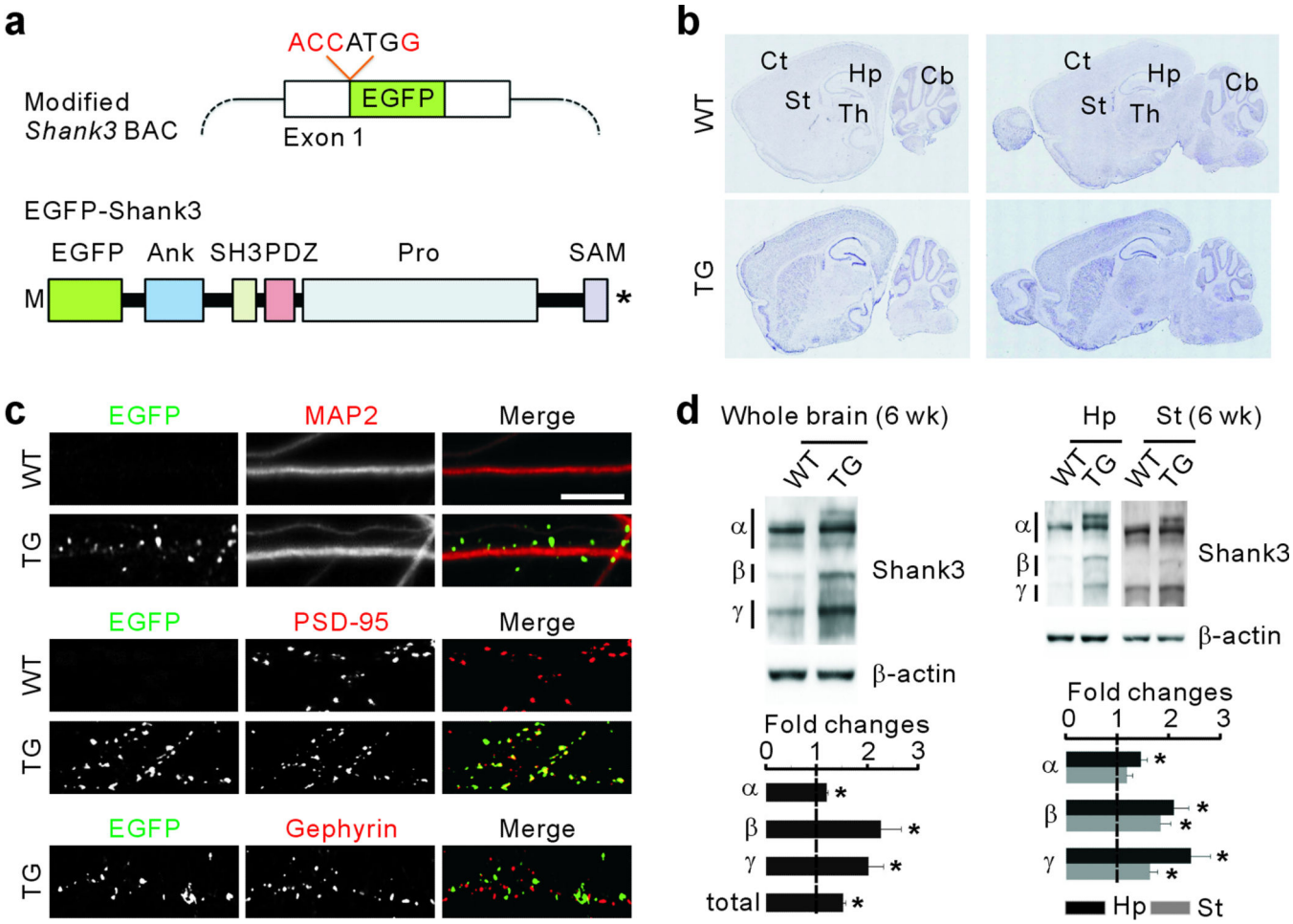

Figure 1. Characterization of EGFP-Shank3 expression in *Shank3* transgenic mice

a, Diagrams show the modified *Shank3* BAC and EGFP-Shank3. Kozak (ACCATGG) and EGFP-coding sequence were integrated into the start codon of *Shank3*. **b**, RNA *in situ* hybridization with a probe against *EGFP* detected *EGFP-Shank3* in the brain. **c**, EGFP-Shank3 localizes to excitatory postsynaptic sites in cultured hippocampal neurons. MAP2 is a dendritic marker. Scale bar, 10 μm. **d**, Quantification of the fold changes of Shank3 (α, β and γ isoforms) in synaptosomal fraction of whole brain (n=4, biological replicates), hippocampus (Hp) or striatum (St) (n=6) from 6-week old (wk) mice. All data are presented as mean ± s.e.m. **P*<0.05; unpaired two-tailed Student's t-test.

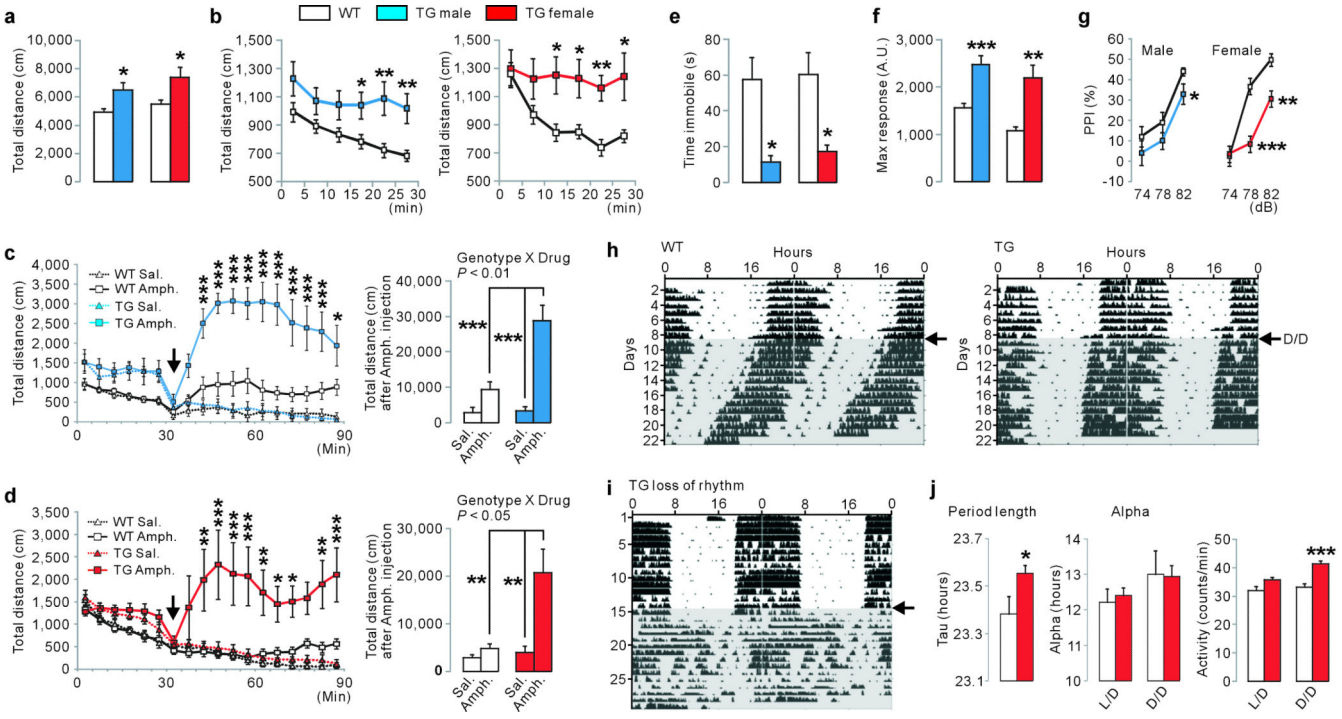

Figure 2. *Shank3* transgenic mice display manic-like behaviors

a, TG mice show increased locomotor activity in the open field test. **b**, TG mice did not habituate during the open field assay. **c,d**, TG mice are hypersensitive to amphetamine. After 30 min of basal activity, amphetamine (2 mg/kg) or saline was administered (arrow) and locomotor activity was monitored for 60 min. **e**, TG mice spend less time immobile in tail-suspension test. **f**, Increased acoustic (120 dB) startle response of TG mice. **g**, Abnormal PPI of TG mice. **h–j**, Abnormal circadian rhythms of TG mice. **h**, Wheel running actograms of WT and TG female mice. After 8 days of light/dark (L/D) cycle, animals were released into constant darkness (arrow, D/D) for 2 weeks. **i**, Among 20 TG mice tested, 3 displayed complete loss of rhythm during D/D. **j**, TG mice showed increased period length and activity count, but normal alpha, compared to WT mice. All data are presented as mean ± s.e.m. **P*<0.05; ***P*<0.01; ****P*<0.001. Statistical analyses for behavioral assays are in Supplementary Table 1.

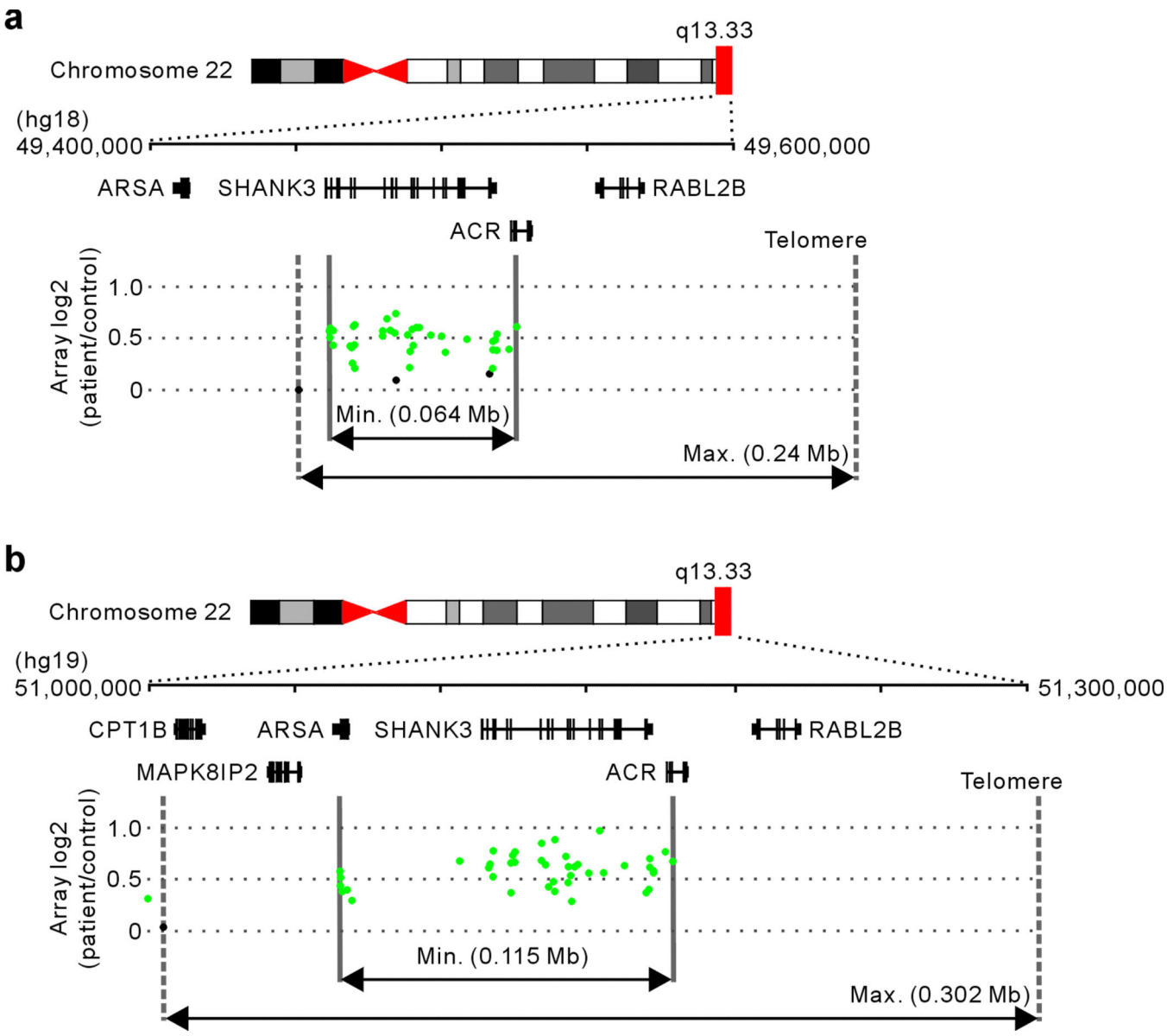

Figure 3. Individuals with *SHANK3* duplications have hyperkinetic disorders

a, Array plot of an exon-targeted chromosome microarray analysis on DNA from an 11-year old female with ADHD, seizures and aberrant behaviors. Black dots indicate probes with normal copy number, while green dots indicate copy number gain. Solid and dotted lines define the minimum and maximum expected boundaries of the duplication, respectively. **b**, Array plot of the 35-year old male with bipolar disorder and epilepsy.

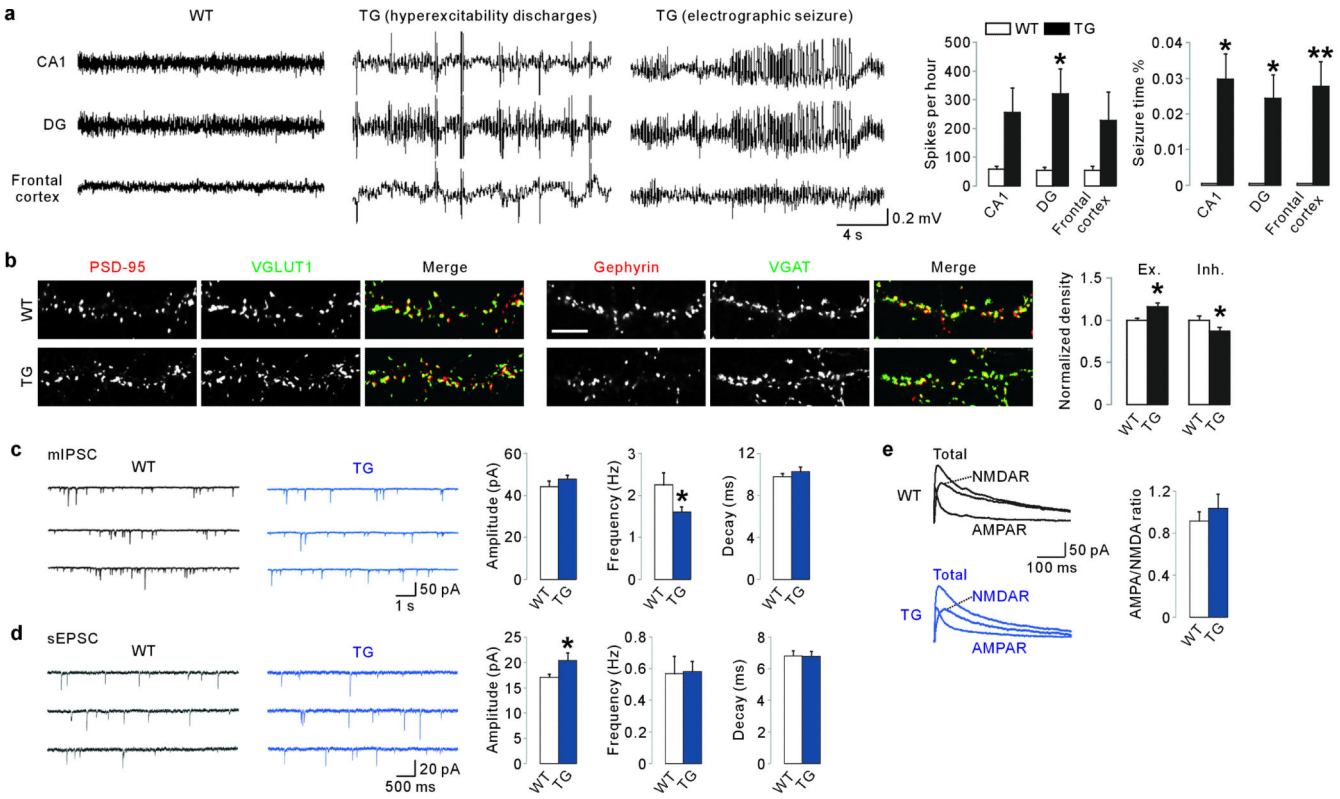

Figure 4. Abnormal EEG and altered synaptic excitatory/inhibitory balance of *Shank3* transgenic mice

a, Representative EEG traces from WT (n=5) and TG (n=10) mice. TG mice showed prolonged hyperexcitability discharges and electrographic seizure in all recorded regions. The frequency of epileptiform spikes (dentate gyrus) and electrographic seizure were significantly increased in TG mice. **b**, Increased VGLUT1-positive PSD-95 (n=28, three independent experiments) and decreased VGAT-positive Gephyrin (n=25) puncta density in cultured hippocampal pyramidal neurons from TG mice. Scale bar, 10 μm. **c**, Frequency, but not amplitude and decay, of mIPSC was decreased in CA1 pyramidal neurons of TG mice (WT n=14, TG n=18). **d**, Amplitude, but not frequency and decay, of sEPSC was increased in TG neurons (n=19). **e**, AMPA/NMDA ratio was normal in TG neurons (n=9). All data are presented as mean ± s.e.m. **P*<0.05; ***P*<0.01. Statistical analyses for these data are in Supplementary Table 2 and 3.

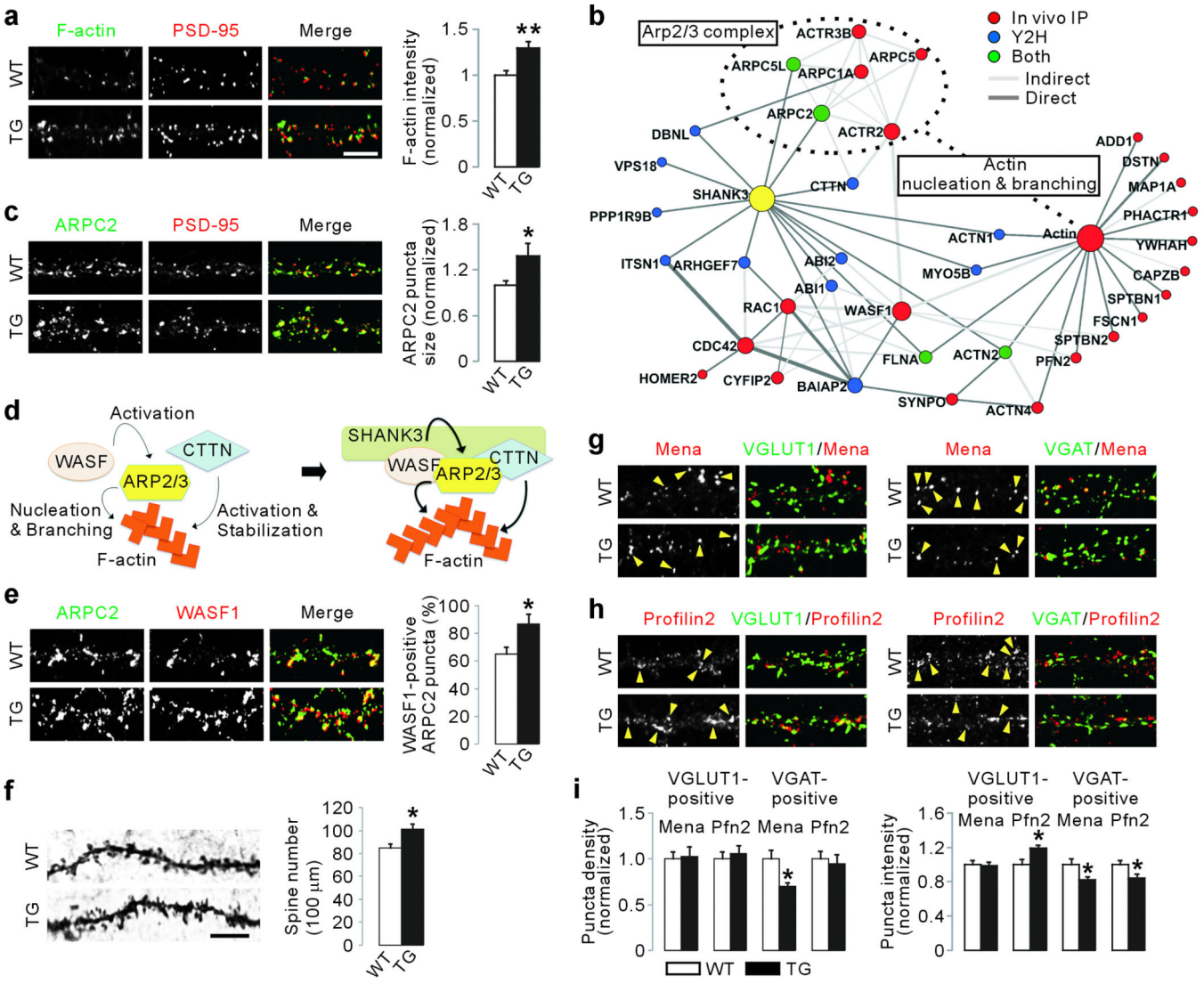

Figure 5. Shank3 interacts directly with Arp2/3 complex to increase F-actin levels in *Shank3* transgenic mice

a, Increased synaptic F-actin in cultured hippocampal pyramidal neurons from TG mice (n=29, three independent experiments). Scale bar, 10 µm. **b**, Actin cytoskeleton-related sub-network of Shank3 interactome. **c**, Increased ARPC2 cluster size in TG pyramidal neurons (n=20). **d**, Diagram shows the proposed role of Shank3 as a platform for F-actin regulating proteins. **e**, Increased co-localization of ARPC2 and WASF1 in TG pyramidal neurons (n=22). **f**, Golgi-staining of CA1 pyramidal neurons shows more dendritic spines in TG mice (n=40 neurons from 3 animals per genotype). **g,h**, Excitatory and inhibitory synaptic distributions of Mena (**g**) and Profilin2 (**h**) in cultured CA1 pyramidal neurons. Yellow arrowheads indicate protein puncta co-localized with corresponding synaptic markers. **i**, Quantification of (**g**) and (**h**). Density of VGAT-positive Mena puncta is decreased in TG neurons (n=18). VGLUT1-positive Profilin2 puncta intensity is increased in TG neurons (n=13), while VGAT-positive Mena and Profilin2 puncta intensity are decreased in TG neurons. All data are presented as mean ± s.e.m. **P*<0.05; ***P*<0.01.

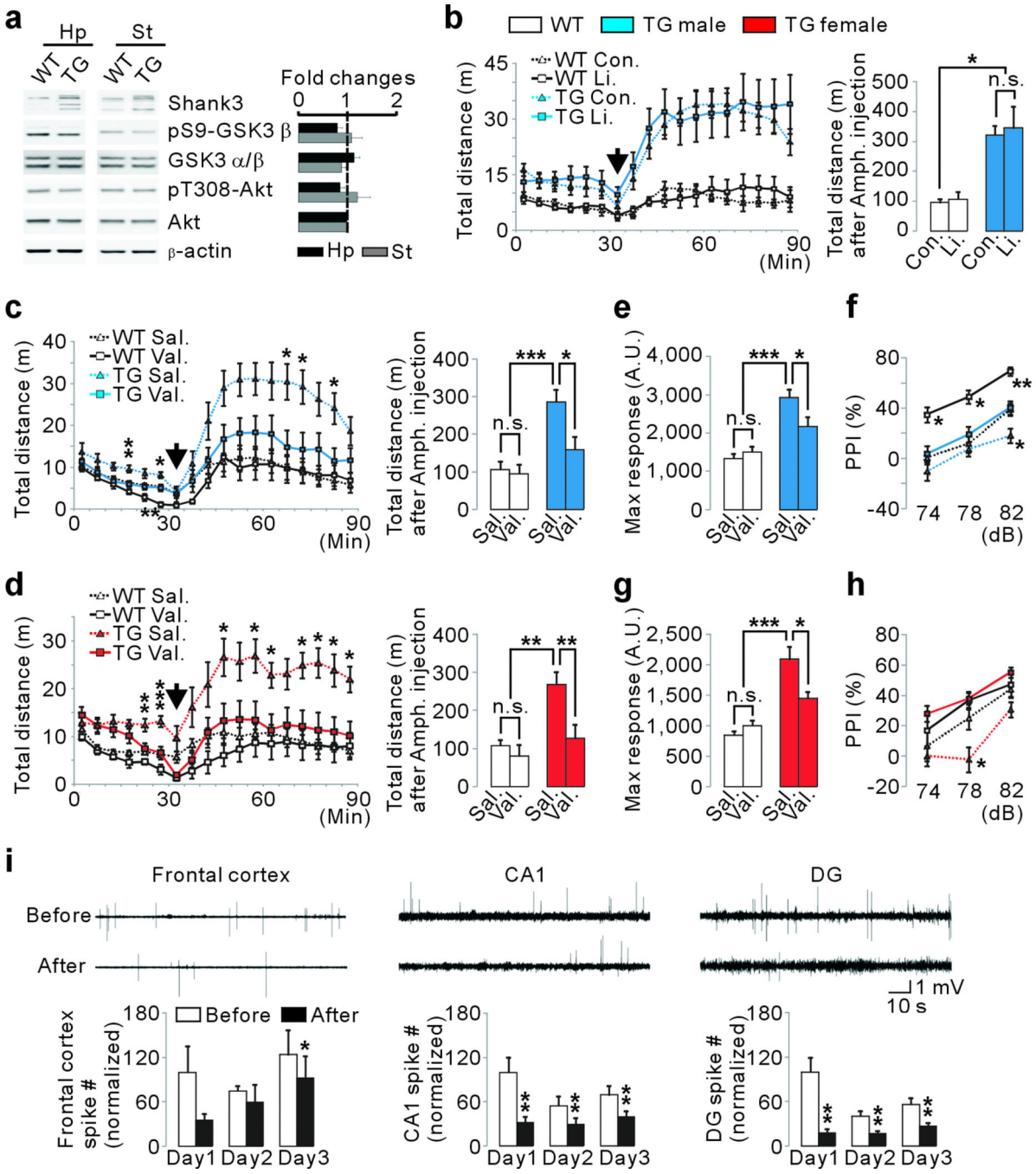

Figure 6. Valproate, but not lithium, rescues manic-like behaviors of *Shank3* transgenic mice

a, Basal activities of GSK-3β and Akt in the hippocampus and striatum of TG mice (10-week old, n=7) are normal. **b**, Amphetamine-sensitivity of male TG mice was not rescued by lithium. **c,d**, Basal locomotor activity and amphetamine-sensitivity of TG mice were rescued by valproate. Basal activity of WT male mice was decreased by valproate during one 5-min time bin. **e–h** Acoustic startle response (**e,g**) and PPI (**f,h**) of TG mice were rescued by valproate. Valproate increased PPI of WT male mice. **i**, Rescue of abnormal EEG in TG mice by valproate. During the three consecutive days of tests, EEG was recorded from the

three brain regions of TG mice (n=7) for one hour before and after valproate injection. Representative EEG traces measured on day 1 are shown. The number of epileptiform spikes was quantified and normalized to the baseline values before treatment of day 1. All data are presented as mean ± s.e.m. **P*<0.05; ***P*<0.01; ****P*<0.001.